BNL-222989-2022-TECH
C-A/AP/660

HJET performance in RHIC Run 22

A. A. Poblaguev

May 2022

Collider Accelerator Department
Brookhaven National Laboratory

U.S. Department of Energy
USDOE Office of Science (SC), Nuclear Physics (NP) (SC-26)

DISCLAIMER

HJET performance in RHIC Run 22

G. Atoian, A. A. Poblaguev,* and A. Zelenski
Brookhaven National Laboratory, Upton, New York 11973, USA
(Dated: May 10, 2022)

In Run 22, the polarized proton beams were resumed at RHIC after four years of heavy ion beam operation. Here we compare HJET performance in the 255 GeV proton Runs 17 and 22. It was found that analyzing power calibration obtained in Run 17 can be used in Run 22 absolute proton beam polarization measurements. Results for average absolute proton beam polarization in the RHIC Run 22 stores are presented.

I. INTRODUCTION

The Relativistic Heavy Ion Collider (RHIC) Spin Program [1] required measurement of the absolute proton beam polarization at 100 – 255 GeV with accuracy better than $\sigma_P/P \lesssim 5\%$ [2]. The Polarized Atomic Hydrogen Gas Jet Target [3] (HJET), commissioned in 2005, had satisfied these requirements by providing $\sigma_P^{\rm syst} P/ \sim 3\%$ precision [4, 5]. After an upgrade of the HJET detectors and data acquisition in 2015 [6], the systematic errors in the absolute polarization measurements were improved to $\sigma_P^{\rm syst}/P \lesssim 0.5\%$ [7]. Consequently, HJET data analysis allowed us to precisely determine [8] elastic proton-proton analyzing power $A_{\rm N}(t)$ for 100 GeV (RHIC Run 15 [9]) and 255 GeV (RHIC Run 17 [10]) .

After a four years break for the heavy ion program, polarized proton beams (255 GeV) were resumed at RHIC. In this note, we advocate that spin correlated asymmetry measurements in Runs 17 and 22 are consistent within $\sim 0.3\%$ (relative) accuracy limited by statistical uncertainties.

Thus, using the *calibrated* analyzing power found in Run 17, online results for the Run 22 beam polarization can be interpreted as final ones, i.e. systematic uncertainties in these measurements do not exceed $\sigma_P^{\rm syst} \lesssim 0.3\%$ (for average beam polarization of about 50% and typical statistical uncertainties of about $\sigma_P^{\rm stat} \sim$ 2–3% per RHIC store).

For each RHIC store in Run 22, online results for the store averaged effective analyzing power and the beam polarization are provided.

II. HJET OPERATION IN RUN 22

HJET was in operation every year since polarized Run 17 during heavy ion RHIC Runs. The primary goal was systematic error study in HJET measurements and experimental evaluation of $p^{\uparrow}$A analyzing power in the forward elastic scattering [7]. In Runs 19 – 21, HJET was also used as a luminescent beam profile monitor for the LEREC [11] development and operation. Several problems in HJET, detectors, electronics, and DAQ operation were identified.

In preparation for polarized Run 22 the major vacuum system upgrades were implemented in collaboration with the Collider-Accelerator Department vacuum group. This ensured reliable HJET vacuum system operation in Run 22. Several problems with the water cooling system were resolved during the Run with minimal HJET downtime.

Noise in detector pre-amplifiers, observed in previous years, was eliminated with all pre-amplifiers board replacements and signal cables refurbishment. As a result, a very stable HJET DAQ operation was demonstrated, which contributed to accurate beam polarization measurements in Run 22.

III. HJET RECOIL SPECTROMETER

The HJET consists of three main parts [3, 7]: *(i)* the atomic beam source (ABS), *(ii)* the recoil proton spectrometer (RPS), and *(iii)* the Breit-Rabi polarimeter (BRP).

ABS provides a vertically polarized ($\sim 96\%$) and vertically directed proton beam (the Jet), which is focused precisely on the collision point, where Jet profile is well approximated by a Gaussian distribution with $\sigma_{\rm jet} \approx 2.6$ mm. Typically, the jet spin is reversed every 5 min.

BRP allows us to precisely determine the jet protons polarization with an accuracy of about 0.1% [3].

RPS is schematically depicted in Fig. 1. The beam protons are scattered off Jet protons. Average verti-

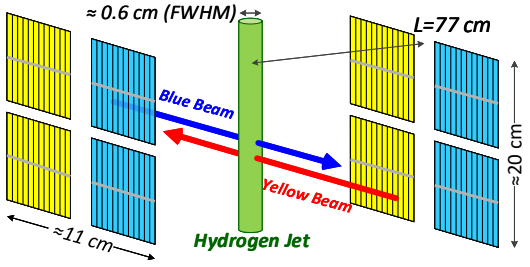

FIG. 1. A schematic view of the HJET recoil spectrometer.

* poblaguev@bnl.gov

cal polarization of both RHIC proton beams, so-called *blue* and *yellow*, with alternatively polarized bunches are measured concurrently and continuously during a RHIC store.

For the elastic forward scattering, the recoil protons are counted in left/right symmetric Si detectors with vertically oriented strips (3.75 mm pitch). For each detected recoil proton, kinetic energy T_R, time of flight $\mathrm{ToF} = t_m - t_0$ (where t_m is the signal time found in the waveform shape fit and t_0 is an offset common for all events in the Si strip), and recoil angle (z-coordinate of the Si strip) are measured.

For the Si detectors used, a recoil proton with kinetic energy above 7.8 MeV punches through the detector and only part of the kinetic energy is visible. However, the signal waveform shape analysis allows us to reconstruct the full kinetic energy of the proton [12].

For elastic proton-proton scattering, there is a strict correlation between the z coordinate of the recoil proton in the detectors and its kinetic energy

$$z - z_{\mathrm{jet}} = L\sqrt{\frac{T_R}{2m_p}\frac{E_{\mathrm{beam}}+m_p}{E_{\mathrm{beam}}-m_p+T_R}} = \zeta_p\sqrt{T_R}. \qquad (1)$$

Here, z_{jet} is the coordinate of the scattering point in the jet (for Jet center, $\langle z_{\mathrm{jet}}\rangle = 0$), $L = 769$ mm is the distance to the detector, E_{beam} is the beam energy, and m_p is a proton mass. For $E_{\mathrm{beam}} = 255$ GeV, $\zeta_p = 17.8\,\mathrm{mm/MeV}^{1/2}$.

A. Determination of the beam absolute polarization

The jet a_{N}^j and beam a_{N}^b spin correlated asymmetries, which can be derived [7] from number of detected elastic events in left/right (LR) detectors discriminated by jet ($+-$) and beam ($\uparrow\downarrow$) spin directions, are proportional to the jet P_{jet} and beam P_{beam} polarization, respectively,

$$a_{\mathrm{N}}^j\left[N_{(LR)}^{(+-)(\uparrow\downarrow)}\right] = A_{\mathrm{N}}^j(T_R)\times P_{\mathrm{jet}}, \qquad (2)$$

$$a_{\mathrm{N}}^b\left[N_{(LR)}^{(+-)(\uparrow\downarrow)}\right] = A_{\mathrm{N}}^b(T_R)\times P_{\mathrm{beam}}. \qquad (3)$$

Analyzing power A_{N} is, generally, a function of the momentum transfer $t = -2m_pT_R$. In HJET measurements, the same events are used to determine a_{N}^j and a_{N}^b. Therefore, for the elastic pp scattering, the jet and beam avarage analyzing powers are expected to be equal, $\langle A_{\mathrm{N}}^j(T_R)\rangle = \langle A_{\mathrm{N}}^b(T_R)\rangle$. Subsequently, the beam polarization can be related to the well determined jet one

$$P_{\mathrm{beam}} = P_{\mathrm{jet}}\,a_{\mathrm{N}}^b/a_{\mathrm{N}}^j, \quad P_{\mathrm{jet}} = 0.957\pm0.001. \qquad (4)$$

So, absolute polarization of the high energy proton beam can be measured with high precision.

As defined in Eqs. (2,3), some essential systematic errors cancel in ratio $a_{\mathrm{N}}^j/a_{\mathrm{N}}^b$ [7]. However, background events may differently alter the jet and beam analyzing powers which can lead to systematic uncertainties in the beam polarization measurements. The following sources of the systematic uncertainties were found [7]:

– *Molecular hydrogen.* The beam scattering off the beam gas hydrogen dilutes the measured a_{N}^j, but does not alter a_{N}^b.

– *pA scattering.* Breakup protons from the beam collision with non-hydrogen ions in the jet and HJET frame. Both, a_{N}^j and a_{N}^j can be affected.

– *Inelastic pp scattering* of the beam proton $p\to\pi X$. Such a background increases a_{N}^b and decreases a_{N}^j [13]. It is kinematically suppressed for 100 GeV beam, but may be essential for 255 GeV.

– *WFT correlated noise.* Weak Field Transition in ABS [3] can induce noise in detectors (preamplifiers). This leads to the detector acceptance dependence on the Jet spin direction and, as a result, may change the measured value of a_{N}^j.

Since for both most intensive backgrounds, *molecular hydrogen* and *pA scattering*, the event rate is about the same in all Si strips, these backgrounds can be subtracted from the elastic data [7]. The systematic corrections to the measured P_{beam} due to *pA scattering* and *WFT correlated noise* can be monitored by variation of the event selection cuts [7].

In Run 17 (255 GeV) data analysis [7], systematic uncertainties in the HJET proton beam polarization measurements were evaluated as

$$\sigma_P^{\mathrm{syst}}/P \lesssim 0.5\% \qquad (5)$$

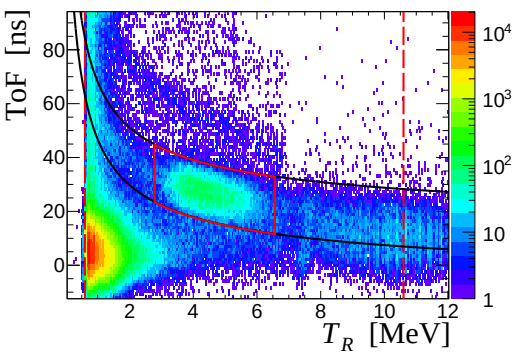

FIG. 2. Time – amplitude distribution of detected signals in a Si strip

B. Elastic events isolation

Typical time-amplitude distribution in a Si strip is shown in Fig. 2.

According to Eq. (1), the energy range of the detected elastic recoil protons is defined by the Si detector geometry. However, to reduce the background rate, additional constraints on T_R are applied by the DAQ trigger

TABLE I. Event selection cuts used Run 17 (255 GeV) data analysis.

Cuts I	Cuts II	
$0.6 < T_R < 10.6$	$2.0 < T_R < 9.5$	MeV
$\lvert\delta t\rvert < 7$	$\lvert\delta t\rvert < 7$	ns
$\left\lvert\delta\sqrt{T}\right\rvert < 0.40$	$-0.18 < \delta\sqrt{T} < 0.30$	$\mathrm{MeV}^{1/2}$

threshold and by the event selection cuts used in the data analysis.

To isolate elastic pp events we should verify that the detected particle is a proton and that the calculated missing mass equals m_p.

To prove that a proton is detected, we can compare the measured time of flight and the kinetic energy:

$$\delta t = \mathrm{ToF} - \frac{L}{c}\sqrt{\frac{m_p}{2T_R}} \approx 0, \tag{6}$$

$$\sqrt{\langle(\delta t)^2\rangle} = \sigma_{\mathrm{bunch}} \sim 2\,\mathrm{ns}, \tag{7}$$

where σ_{bunch} is rms longitudinal size of the beam bunch.

Since the inelastic scattering invalidates Eq. (1), a comparison of the measured $\sqrt{T_R}$ with the Si strip z-coordinate allows us to isolate the elastic events:

$$\delta\sqrt{T} = \sqrt{T_R} - z_{\mathrm{strip}}/\zeta_p \approx 0, \tag{8}$$

$$\sqrt{\langle(\delta\sqrt{T_R})^2\rangle} = \sigma_{\mathrm{jet}}/\zeta_p \sim 0.14\,\mathrm{MeV}^{1/2}, \tag{9}$$

where σ_{jet} is rms geometrical thickness of the jet.

It is important to point out that the same δt and $\delta\sqrt{T_R}$ event selection cuts can be used for all HJET Si strips.

In the Run 17 data analysis [7], two main sets of event selection cuts (see Table I) were used. The first one (Cuts I) accepts as many elastic events as reasonably possible to minimize the statistical uncertainty in the measurements. The second set (Cuts II) minimizes uncontrollable systematic corrections.

C. Calibrated analyzing power for Cuts I

In Run 17, systematic corrections to the measured beam polarization were thoroughly studied for Cuts II. Using the results obtained, we found the *calibrated* analyzing power [7] for *blue* (B) and *yellow* (Y) beams:

$$\left(A_N^{\mathrm{cal}}\right)_{\mathrm{B}} = 3.749 \pm 0.013_{\mathrm{stat}} \pm 0.014_{\mathrm{syst}}\,\%, \tag{10}$$

$$\left(A_N^{\mathrm{cal}}\right)_{\mathrm{Y}} = 3.739 \pm 0.012_{\mathrm{stat}} \pm 0.014_{\mathrm{syst}}\,\%, \tag{11}$$

which can be used with Cuts I events selection to determine the beam polarization

$$P_{\mathrm{beam}} = a_{\mathrm{N}}^{b}(\mathrm{Cuts\,I}) \,/\, A_{\mathrm{N}}^{\mathrm{cal}}. \tag{12}$$

For such a determination of P_{beam}, both, statistical and systematic, uncertainties are minimized. For an 8 h store

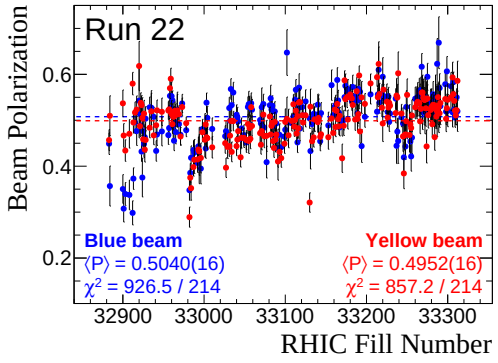

FIG. 3. Online measurements of the *blue* and *yellow* proton beam polarization in RHIC Run 22. The shown numbers are results of the zero degree polynomial fit (dashed lines).

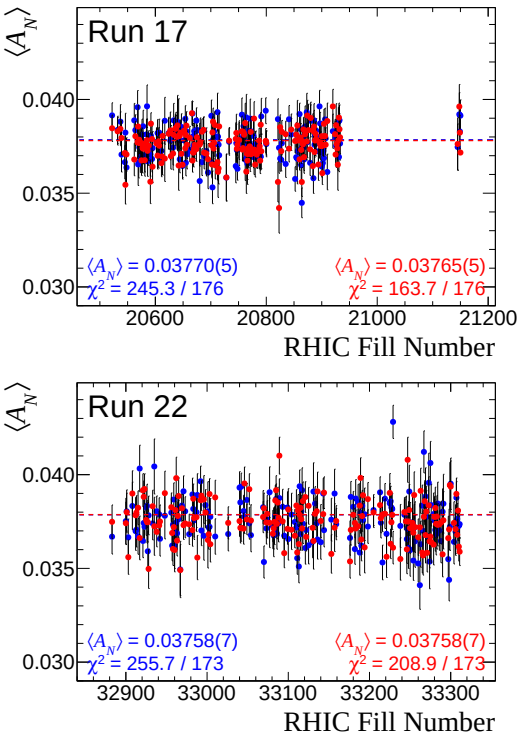

FIG. 4. The measured effective analyzing power (Cuts I) in Runs 17 and 22.

in Run 17, typical result for the 255 GeV beam polarization measurement was [7, 8]

$$P_{\mathrm{beam}} = (56 \pm 2.0_{\mathrm{stat}} \pm 0.3_{\mathrm{syst}})\,\%. \tag{13}$$

IV. ONLINE DATA ANALYSIS IN RUN 22

Since RPS was not altered between RHIC Runs 17 and 22, for online determination of the beam polarization in

TABLE II. Comparison of the average single $a_{\rm N}^b$, $a_{\rm N}^j$ and double $a_{\rm NN}$ spin asymmetries in Runs 17 and 22. Since asymmetry b_{NN}, defined in Ref. [7], is expected to be identical to 0, it may be used to search for systematic errors in the measurements. Only the stores with the holding field magnet [3] switched on and $N_{\rm el}^{\rm tot} > 1.0$ (Fig. 6) were considered.

		Run 22		**Run 17**		Results consitency
		Blue beam	*Yellow* beam	*Blue* beam	*Yellow* beam	χ^2/ndf
$\langle P_{\rm beam}\rangle = a_{\rm N}^b/A_{\rm N}^{\rm cal}$	[%]	50.0 ± 0.18	49.5 ± 0.18	55.3 ± 0.15	56.1 ± 0.14	
$\langle A_{\rm N}\rangle = a_{\rm N}^j/P_{\rm jet}$	[%]	3.757 ± 0.007	3.757 ± 0.007	3.769 ± 0.006	3.765 ± 0.006	2.6 / 3
$\langle A_{\rm NN}\rangle = a_{\rm NN}/P_{\rm jet}P_{\rm beam}$	[%]	0.050 ± 0.015	0.063 ± 0.015	0.076 ± 0.009	0.073 ± 0.009	2.5 / 3
$\langle b_{\rm NN}\rangle$	[%]	-0.003 ± 0.007	-0.003 ± 0.007	-0.003 ± 0.006	0.000 ± 0.005	0.8 / 4

TABLE III. The ratio of single spin asymmetries $a_{\rm N}$ determined with and without background subtraction.

	Jet asymmetry $a_{\rm N}^j$		Beam asymmetry $a_{\rm N}^b$	
	Blue	*Yellow*	*Blue*	*Yellow*
Run 22	1.156	1.155	1.125	1.117
Run 17	1.067	1.068	1.049	1.044

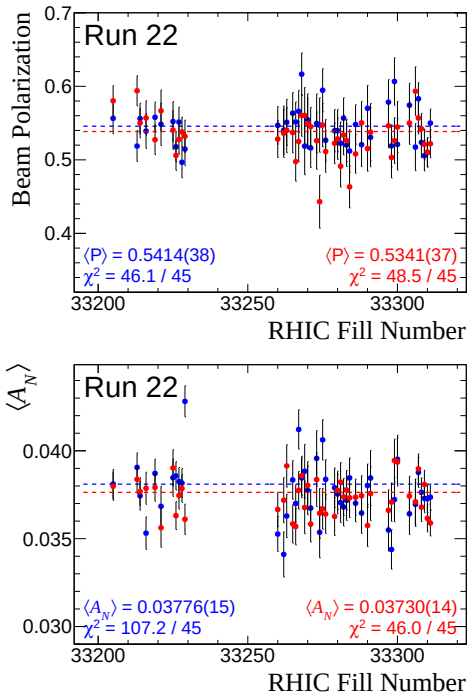

FIG. 5. Measured beam polarization and analyzing power for the stable polarization stores

Run 22 we have used event selection Cuts I and *calibrated* analyzing powers given by central values in Eqs. (10,11). Explanation of the calculations and detailed, RHIC store by store, results are given in Appendix A. The measured, store averaged, absolute polarization of RHIC *blue* and *yellow* beams in Run 22 Fills are depicted in Fig. 3.

To verify that effective analyzing powers found in Run 17 can be used in Run 22 measurements, we can compare (see Fig. 4) values of $A_{\rm N}$ measured in these RHIC Runs. One can see that all four Run averaged analyzing powers are in reasonable agreement within relative statistical uncertainties of about 0.2%.

It should be noted that for *blue* beam χ^2/ndf ratio is noticeably larger than 1. However, according to Ref. [7], this does not affect the interpretation of the results of the beam polarization measurements. If the excess of χ^2 can be attributed to an instability of the systematic corrections, then the effect can be approximated by about a 20% (relative) increase in the statistical uncertainty.

To compare the stability of the measurements of the jet $a_{\rm N}^j$ and beam $a_{\rm N}^b$ asymmetries, we selected RHIC Fills, 33205 – 33229 and 33260 - 33312 with approximately stable beam polarization (see Fig. 5). For the beam polarization, $\chi^2/{\rm ndf} \approx 1$, while for the *blue* beam analyzing power $\chi^2/{\rm ndf} = 2.4 \pm 0.2$. Even if Fill 33229 with an anomalously large value of $A_{\rm N}$ is excluded from the fit, then $\chi^2/{\rm ndf} = 73.6/44$, which corresponds to a 3.2 standard deviation discrepancy.

Thus, the results shown in Fig. 5 suggest that increased χ^2 in the $A_{\rm N}$ fit is not directly relevant to the beam polarization measurements. For example, such a situation can be caused by fluctuations of the systematic uncertainties due to *molecular hydrogen* background or due to *WFT correlated noise*.

It must be pointed out that, since relative statistical uncertainties for $P_{\rm beam}$ ($a_{\rm N}^b$) are about factor 2 larger than for $A_{\rm N}$ ($a_{\rm N}^j$), the conclusion made cannot be considered unambiguous. Nonetheless,

– a similar effect was also observed in Run 17;

– in the beam polarization measurements, there is no evidence of systematic error fluctuations.

The measured values of single $A_{\rm N}$ and double $A_{\rm NN}$ analyzing powers must be Run year and RHIC ring independent. Although these values found in Run 17 are systematically lower than those in Run 22 (see Table II), the discrepancy cannot be interpreted as statistically significant.

To evaluate elastic data contamination by background events, one can consider the ratio of the single spin asymmetries determined with and without background subtraction (see Table III). Since *molecular hydrogen* background does not affect the beam asymmetry measure-

ment, we can easily evaluate this background fraction as $\sim 2\%$ (Run 17) and $\sim 3.5\%$ (Run 22). For *pA scattering* background fraction, we find $\sim 4.5\%$ (Run 17) and $\sim 12\%$ (Run 22). It should be noted that the fractions are given for recoil proton energies range $0.6 < T_R < 10.6$ MeV. Increasing the lower limit for T_R leads to fast dilution of the background fraction.

V. SUMMARY

For online determination of the RHIC 255 GeV proton beam polarization in Run 22, we have used *calibrated*, i.e. including systematic corrections, analyzing power determined in the offline analysis [7] of the Run 17 data. Since the measured analyzing powers in Runs 17 and 22 appeared to be the same within $\sim 0.2\%$ statistical uncertainty, we can conclude that Run 17 evaluation of the systematic uncertainties (5) is also valid for Run 22 online measurements.

Although the background fraction in the elastic data in Run 22 is about factor 2.3 (or by about 9% in absolute units) larger than in Run 17, the measured analyzing power was not altered. This result may be interpreted as a proof that the background subtraction method works sufficiently well. Uncertainty in the evaluation of the background fraction does not exceed 3–4% of the background rate.

Thus, we found that HJET provides stable and accurate determination of the proton beam absolute polarization at RHIC energies. Precision of the online measurements in Run 22 fully satisfies the requirements for absolute calibration of the proton beam polarization at RHIC.

In further Run 22 data analysis, we consider independent evaluation of the *calibrated* analyzing power for these measurements as well as determination of the hadronic spin-flip amplitude parameter r_5 [8, 14].

In the preparation for the next polarized Run 24 we plan to upgrade the dissociator cooling system with the new cold head to improve ABS operation stability at the high atomic beam intensity. The HJET will be also used as the beam profile monitor for the LEREC APEX studies in Run 23.

Appendix A: HJET online results for the 255 GeV proton beam polarization measurements in Run 22

For each RHIC store, analyzing power $\langle A_{\rm N}\rangle$ and beam polarization $\langle P_{\rm beam}\rangle$ were derived online from the measured, using Cuts I, target $a_{\rm N}^j$ and beam $a_{\rm N}^b$ spin correlated asymmetries

$$\langle A_{\rm N}\rangle = a_{\rm N}^j/P_{\rm jet}, \quad P_{\rm jet}=95.7\%, \tag{A1}$$

$$\langle P_{\rm beam}\rangle = a_{\rm N}^b/A_{\rm N}^B, \quad A_{\rm N}^B=3.749\% \ (\textit{Blue} \text{ beam}), \tag{A2}$$

$$\langle P_{\rm beam}\rangle = a_{\rm N}^b/A_{\rm N}^Y, \quad A_{\rm N}^Y=3.739\% \ (\textit{Yellow} \text{ beam}), \tag{A3}$$

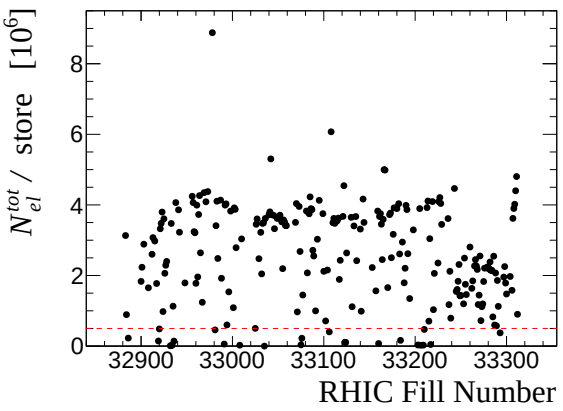

FIG. 6. Good (elastic *pp*) event statistics per Run 22 RHIC store. The dashed line shows the threshold value (0.5) used to select RHIC Fills for the calculation of $\langle P_{\rm beam}\rangle$.

where *calibrated* analyzing powers $A_{\rm N}^B$ and $A_{\rm N}^Y$ are taken from Eqs. (10,11).

As defined, $\langle A_{\rm N}\rangle$ is directly evaluated (no systematic corrections applied) analyzing power averaged over detector acceptance and momentum transfer $t=-2m_pT_R$ range corresponding to $0.6 < T_R < 10.6$ MeV, while $\langle P_{\rm beam}\rangle$ is the beam profile and RHIC store averaged vertical component of the beam polarization (after systematic corrections).

The results for Run 22 stores (Fills) with total statistics $N_{\rm el}^{\rm tot} > 0.5$ (see Fig. 6) are summarized in Table IV. During some stores the HJET holding field magnet [3] was switched off and, consequently, the jet polarization was not well defined. Therefore, $\langle A_{\rm N}\rangle$ was not calculated for these stores.

Run 22 averaged values of $\langle A_{\rm N}\rangle$ and $\langle P_{\rm beam}\rangle$ were obtained by combining all stores data into one data sample. To calculate average $\langle A_{\rm N}\rangle$, only Fills with $N_{\rm el}^{\rm tot} > 1.0$ were used. For comparison, similarly calculated Run 17 values are also shown.

TABLE IV: Online determined values of $\langle A_N \rangle$ and $\langle P_{beam} \rangle$ for Run 22 stores. Only statistical uncertainties are shown. For $\langle P_{beam} \rangle$, the systematic uncertainty is evaluated as $\sigma^{syst} P \approx 0.3\%$.

RHIC Fill	***Blue* beam** $\langle A_N \rangle$ [%]	$\langle P_{beam} \rangle$[%]	***Yellow* beam** $\langle A_N \rangle$ [%]	$\langle P_{beam} \rangle$[%]
32883	3.669 ± 0.092	44.9 ± 2.4	3.748 ± 0.090	45.7 ± 2.3
32884	3.429 ± 0.171	35.7 ± 4.4	4.012 ± 0.171	51.0 ± 4.3
32900	3.752 ± 0.123	35.0 ± 3.1	3.741 ± 0.114	53.7 ± 2.9
32901	3.804 ± 0.114	30.8 ± 2.9	3.800 ± 0.101	46.7 ± 2.6
32903	3.666 ± 0.098	34.0 ± 2.5	3.560 ± 0.092	43.4 ± 2.3
32908	3.833 ± 0.127	33.7 ± 3.2	3.900 ± 0.121	47.0 ± 3.1
32912	3.699 ± 0.103	29.8 ± 2.6	3.783 ± 0.096	58.0 ± 2.5
32913	3.706 ± 0.093	37.3 ± 2.4	3.797 ± 0.091	49.5 ± 2.3
32915	3.671 ± 0.096	49.5 ± 2.4	3.823 ± 0.090	51.7 ± 2.3
32917	4.033 ± 0.124	47.7 ± 3.2	3.662 ± 0.117	52.3 ± 3.0
32920	3.664 ± 0.317	54.3 ± 8.1	3.574 ± 0.209	61.8 ± 5.4
32921	3.646 ± 0.089	51.4 ± 2.3	3.917 ± 0.089	48.7 ± 2.3
32922	3.742 ± 0.088	48.9 ± 2.2	3.882 ± 0.086	53.8 ± 2.2
32923	3.722 ± 0.085	43.2 ± 2.2	3.923 ± 0.081	53.3 ± 2.1
32924	3.916 ± 0.166	37.5 ± 4.2	3.717 ± 0.171	50.5 ± 4.4
32925	3.825 ± 0.088	47.6 ± 2.3	3.758 ± 0.082	45.9 ± 2.1
32926	3.834 ± 0.115	44.8 ± 2.9	3.748 ± 0.113	51.4 ± 2.9
32927	3.591 ± 0.108	46.3 ± 2.8	3.746 ± 0.106	43.6 ± 2.7
32928	3.783 ± 0.103	50.4 ± 2.6	3.498 ± 0.105	45.7 ± 2.7
32933	3.740 ± 0.088	52.8 ± 2.3	3.832 ± 0.086	48.4 ± 2.2
32935	4.044 ± 0.147	52.7 ± 3.7	3.725 ± 0.155	51.9 ± 3.9
32938	3.805 ± 0.082	50.7 ± 2.1	3.695 ± 0.080	46.7 ± 2.0
32941	3.789 ± 0.088	43.3 ± 2.2	3.729 ± 0.077	48.9 ± 2.0
32942	3.658 ± 0.092	46.9 ± 2.3	3.750 ± 0.088	52.2 ± 2.2
32948	3.781 ± 0.123	47.6 ± 3.1	3.901 ± 0.117	51.8 ± 3.0
32956	3.797 ± 0.080	46.8 ± 2.1	3.826 ± 0.076	52.1 ± 2.0
32957	3.621 ± 0.081	48.3 ± 2.1	3.689 ± 0.078	52.4 ± 2.0
32958	3.733 ± 0.089	55.3 ± 2.3	3.604 ± 0.088	57.0 ± 2.3
32959	3.867 ± 0.089	52.8 ± 2.3	3.720 ± 0.090	59.0 ± 2.3
32960	3.622 ± 0.123	55.2 ± 3.1	3.598 ± 0.117	51.3 ± 3.0
32961	3.694 ± 0.080	54.3 ± 2.1	3.811 ± 0.080	49.1 ± 2.1
32962	3.744 ± 0.116	48.8 ± 3.0	3.982 ± 0.112	50.8 ± 2.8
32963	3.687 ± 0.085	45.5 ± 2.2	3.648 ± 0.081	50.9 ± 2.1
32964	3.819 ± 0.082	49.6 ± 2.1	3.780 ± 0.075	52.1 ± 1.9
32965	3.763 ± 0.101	47.4 ± 2.6	3.886 ± 0.097	51.1 ± 2.5
32967	3.494 ± 0.150	52.3 ± 3.8	3.491 ± 0.136	52.1 ± 3.5
32969	3.835 ± 0.080	49.2 ± 2.0	3.821 ± 0.075	51.3 ± 1.9
32971	3.911 ± 0.083	46.8 ± 2.1	3.731 ± 0.077	46.5 ± 2.0
32973	3.805 ± 0.078	53.7 ± 2.0	3.740 ± 0.077	52.9 ± 2.0
32978	3.682 ± 0.055	47.8 ± 1.4	3.735 ± 0.054	49.4 ± 1.4
32982	3.894 ± 0.087	34.8 ± 2.2	3.704 ± 0.086	28.9 ± 2.2
32983	3.817 ± 0.081	38.5 ± 2.1	3.872 ± 0.078	37.5 ± 2.0
32984	3.756 ± 0.102	41.8 ± 2.6	3.769 ± 0.102	35.2 ± 2.6
32987	3.799 ± 0.081	43.5 ± 2.1	3.773 ± 0.077	39.8 ± 2.0
32988	3.892 ± 0.114	42.9 ± 2.9	3.558 ± 0.118	41.4 ± 3.0
32992	3.965 ± 0.081	40.7 ± 2.1	3.864 ± 0.080	41.5 ± 2.0
32993	3.702 ± 0.081	44.3 ± 2.1	3.888 ± 0.080	43.6 ± 2.0
32994	4.128 ± 0.210	41.6 ± 5.4	3.073 ± 0.204	43.2 ± 5.2
32996	3.674 ± 0.130	39.5 ± 3.3	3.868 ± 0.127	41.8 ± 3.3
32998	3.838 ± 0.083	48.1 ± 2.1	3.798 ± 0.081	47.4 ± 2.1
33001	3.805 ± 0.158	47.4 ± 4.0	3.652 ± 0.150	45.8 ± 3.8
33002	3.718 ± 0.083	43.9 ± 2.1	3.682 ± 0.080	49.1 ± 2.0
33003	3.722 ± 0.083	53.8 ± 2.1	3.897 ± 0.082	46.3 ± 2.1
33004	3.775 ± 0.098	50.5 ± 2.5	3.629 ± 0.095	46.1 ± 2.4
33010	3.670 ± 0.094	48.1 ± 2.4	3.879 ± 0.091	44.1 ± 2.3

continued on next page

TABLE IV *(continued)*

RHIC Fill	***Blue* beam** $\langle A_N \rangle$ [%]	$\langle P_{beam} \rangle$[%]	***Yellow* beam** $\langle A_N \rangle$ [%]	$\langle P_{beam} \rangle$[%]
33026	3.683 ± 0.090	46.5 ± 2.3	3.743 ± 0.086	45.0 ± 2.2
33027	—	47.6 ± 2.3	—	39.7 ± 2.1
33029	—	46.9 ± 2.7	—	44.2 ± 2.5
33031	—	52.7 ± 2.4	—	44.4 ± 2.2
33032	—	49.9 ± 3.0	—	46.6 ± 2.7
33033	—	56.8 ± 2.2	—	49.9 ± 2.2
33034	—	53.3 ± 2.3	—	43.1 ± 2.2
33036	—	56.0 ± 2.2	—	49.8 ± 2.1
33040	3.931 ± 0.085	51.2 ± 2.2	3.752 ± 0.083	44.4 ± 2.1
33041	3.852 ± 0.085	50.7 ± 2.2	3.717 ± 0.081	45.8 ± 2.1
33042	3.936 ± 0.072	49.7 ± 1.8	3.714 ± 0.070	47.6 ± 1.8
33045	3.806 ± 0.085	46.0 ± 2.2	3.712 ± 0.083	41.9 ± 2.1
33046	3.776 ± 0.090	48.2 ± 2.3	3.953 ± 0.088	46.2 ± 2.2
33049	3.865 ± 0.088	46.8 ± 2.2	3.761 ± 0.082	46.2 ± 2.1
33052	3.741 ± 0.085	45.2 ± 2.2	3.922 ± 0.083	45.7 ± 2.1
33054	3.677 ± 0.088	52.9 ± 2.3	3.756 ± 0.083	49.2 ± 2.1
33055	—	53.5 ± 2.8	—	45.5 ± 2.7
33056	—	53.1 ± 2.2	—	48.3 ± 2.1
33057	—	49.0 ± 2.2	—	46.0 ± 2.2
33058	—	53.7 ± 2.2	—	52.9 ± 2.2
33059	—	52.3 ± 2.3	—	48.8 ± 2.2
33069	3.826 ± 0.089	50.1 ± 2.3	3.774 ± 0.084	47.2 ± 2.1
33070	3.534 ± 0.086	49.3 ± 2.2	3.821 ± 0.080	44.7 ± 2.1
33071	3.807 ± 0.166	52.8 ± 4.2	3.743 ± 0.160	47.6 ± 4.1
33073	3.713 ± 0.084	53.5 ± 2.1	3.745 ± 0.079	51.2 ± 2.0
33074	3.762 ± 0.100	48.4 ± 2.5	3.791 ± 0.099	46.6 ± 2.5
33077	3.906 ± 0.136	40.9 ± 3.5	3.743 ± 0.132	46.6 ± 3.4
33081	3.726 ± 0.085	53.3 ± 2.2	3.685 ± 0.080	50.8 ± 2.1
33082	3.675 ± 0.113	54.8 ± 2.9	3.714 ± 0.110	46.9 ± 2.8
33083	3.711 ± 0.084	52.3 ± 2.1	3.748 ± 0.081	48.8 ± 2.1
33084	3.780 ± 0.086	53.2 ± 2.2	3.863 ± 0.081	49.4 ± 2.1
33085	3.870 ± 0.080	46.9 ± 2.0	3.917 ± 0.078	45.5 ± 2.0
33086	3.686 ± 0.083	48.8 ± 2.1	3.739 ± 0.080	44.0 ± 2.1
33087	3.766 ± 0.083	51.9 ± 2.1	3.852 ± 0.081	49.7 ± 2.1
33088	3.740 ± 0.099	45.6 ± 2.5	3.771 ± 0.097	45.8 ± 2.5
33089	3.875 ± 0.103	49.3 ± 2.6	4.101 ± 0.099	46.9 ± 2.5
33091	3.673 ± 0.163	43.9 ± 4.2	3.603 ± 0.159	41.0 ± 4.1
33093	3.828 ± 0.094	46.8 ± 2.4	3.751 ± 0.092	43.1 ± 2.3
33095	3.674 ± 0.082	44.1 ± 2.1	3.581 ± 0.078	41.8 ± 2.0
33099	3.825 ± 0.085	46.4 ± 2.2	3.711 ± 0.083	44.9 ± 2.1
33100	3.657 ± 0.113	47.9 ± 2.9	3.814 ± 0.111	49.6 ± 2.8
33102	3.557 ± 0.195	64.7 ± 5.0	3.466 ± 0.186	50.3 ± 4.8
33104	3.787 ± 0.114	49.5 ± 2.9	3.706 ± 0.106	46.7 ± 2.7
33108	3.747 ± 0.068	49.4 ± 1.7	3.674 ± 0.065	49.9 ± 1.7
33110	3.718 ± 0.089	50.8 ± 2.3	3.835 ± 0.085	53.5 ± 2.2
33111	3.555 ± 0.086	50.1 ± 2.2	3.585 ± 0.084	48.6 ± 2.1
33112	3.721 ± 0.090	54.5 ± 2.3	3.809 ± 0.085	50.0 ± 2.2
33113	3.510 ± 0.087	56.6 ± 2.2	3.630 ± 0.085	52.1 ± 2.2
33114	3.938 ± 0.087	54.2 ± 2.2	3.786 ± 0.086	47.1 ± 2.2
33115	3.683 ± 0.087	45.2 ± 2.2	3.823 ± 0.085	50.9 ± 2.2
33116	3.803 ± 0.086	52.6 ± 2.2	3.762 ± 0.084	48.3 ± 2.2
33117	3.917 ± 0.119	57.1 ± 3.0	3.713 ± 0.116	53.9 ± 3.0
33118	3.738 ± 0.105	48.2 ± 2.7	3.859 ± 0.102	54.0 ± 2.6
33121	3.609 ± 0.087	52.9 ± 2.2	3.881 ± 0.082	51.1 ± 2.1
33122	3.705 ± 0.077	51.1 ± 2.0	3.668 ± 0.075	49.5 ± 1.9
33125	3.623 ± 0.100	54.1 ± 2.5	3.834 ± 0.098	51.1 ± 2.5
33130	3.642 ± 0.086	50.4 ± 2.2	3.717 ± 0.083	32.1 ± 2.1
33131	3.910 ± 0.154	43.3 ± 3.9	3.646 ± 0.150	53.0 ± 3.8
33133	3.846 ± 0.090	49.2 ± 2.3	3.791 ± 0.085	45.4 ± 2.2

continued on next page

TABLE IV *(continued)*

RHIC Fill	***Blue* beam** $\langle A_N \rangle$ [%]	$\langle P_{beam} \rangle$[%]	***Yellow* beam** $\langle A_N \rangle$ [%]	$\langle P_{beam} \rangle$[%]
33135	3.740 ± 0.087	51.4 ± 2.2	3.805 ± 0.082	46.3 ± 2.1
33136	3.654 ± 0.105	50.3 ± 2.7	3.911 ± 0.103	50.2 ± 2.6
33140	3.640 ± 0.091	53.4 ± 2.3	3.753 ± 0.088	49.6 ± 2.2
33141	4.127 ± 0.163	51.4 ± 4.1	3.927 ± 0.161	50.5 ± 4.1
33143	3.899 ± 0.082	45.4 ± 2.1	3.789 ± 0.077	46.4 ± 2.0
33144	3.704 ± 0.089	51.6 ± 2.3	3.904 ± 0.084	46.9 ± 2.2
33153	3.760 ± 0.114	48.9 ± 2.9	3.577 ± 0.103	46.3 ± 2.6
33157	3.899 ± 0.130	57.7 ± 3.3	3.717 ± 0.128	50.4 ± 3.3
33159	3.736 ± 0.083	51.1 ± 2.1	3.753 ± 0.082	47.2 ± 2.1
33161	—	52.9 ± 2.2	—	52.3 ± 2.1
33162	—	53.3 ± 2.1	—	48.5 ± 2.1
33163	—	52.5 ± 2.2	—	52.1 ± 2.2
33164	—	58.8 ± 2.7	—	53.6 ± 2.6
33165	—	54.3 ± 2.2	—	50.2 ± 2.2
33166	—	51.6 ± 1.9	—	48.7 ± 1.8
33167	—	48.5 ± 1.9	—	51.0 ± 1.8
33170	—	49.8 ± 3.3	—	41.7 ± 3.1
33172	—	50.0 ± 2.1	—	48.8 ± 2.1
33173	—	55.0 ± 2.1	—	58.7 ± 2.1
33174	—	57.5 ± 2.6	—	54.6 ± 2.5
33176	3.663 ± 0.092	56.4 ± 2.3	3.537 ± 0.089	55.0 ± 2.3
33177	3.881 ± 0.083	56.8 ± 2.1	3.705 ± 0.081	50.2 ± 2.1
33180	3.828 ± 0.082	55.6 ± 2.1	3.786 ± 0.081	55.6 ± 2.1
33182	3.603 ± 0.081	54.2 ± 2.1	3.742 ± 0.080	54.7 ± 2.0
33183	3.873 ± 0.101	57.3 ± 2.6	3.713 ± 0.098	53.3 ± 2.5
33186	3.854 ± 0.095	55.2 ± 2.4	3.725 ± 0.092	50.2 ± 2.4
33188	3.584 ± 0.121	54.2 ± 3.1	3.835 ± 0.119	56.3 ± 3.0
33189	3.796 ± 0.109	51.5 ± 2.8	3.983 ± 0.107	50.4 ± 2.7
33190	3.622 ± 0.082	56.8 ± 2.1	3.654 ± 0.080	51.3 ± 2.0
33191	3.834 ± 0.083	54.6 ± 2.1	3.779 ± 0.081	59.8 ± 2.1
33192	3.758 ± 0.099	56.2 ± 2.5	3.890 ± 0.100	47.6 ± 2.5
33194	3.789 ± 0.140	44.4 ± 3.6	3.612 ± 0.136	55.0 ± 3.5
33198	3.723 ± 0.089	50.8 ± 2.3	3.870 ± 0.088	53.6 ± 2.2
33205	3.811 ± 0.083	55.6 ± 2.1	3.798 ± 0.081	58.0 ± 2.1
33213	3.906 ± 0.083	51.9 ± 2.1	3.838 ± 0.080	59.4 ± 2.1
33214	3.744 ± 0.081	55.6 ± 2.1	3.768 ± 0.078	55.0 ± 2.0
33215	3.849 ± 0.194	61.0 ± 5.0	3.874 ± 0.188	62.3 ± 4.8
33216	3.532 ± 0.093	53.9 ± 2.4	3.787 ± 0.091	55.7 ± 2.3
33219	3.872 ± 0.081	55.8 ± 2.1	3.792 ± 0.079	52.7 ± 2.0
33220	3.845 ± 0.163	59.5 ± 4.2	3.714 ± 0.154	49.3 ± 3.9
33221	3.684 ± 0.113	54.8 ± 2.9	3.562 ± 0.111	56.7 ± 2.8
33225	3.847 ± 0.106	55.2 ± 2.7	3.903 ± 0.103	54.0 ± 2.6
33226	3.857 ± 0.081	51.8 ± 2.1	3.631 ± 0.079	50.6 ± 2.0
33227	3.825 ± 0.080	55.1 ± 2.0	3.746 ± 0.078	52.8 ± 2.0
33228	3.817 ± 0.082	49.7 ± 2.1	3.785 ± 0.078	53.8 ± 2.0
33229	4.281 ± 0.088	51.5 ± 2.3	3.611 ± 0.086	53.2 ± 2.2
33236	—	54.7 ± 2.2	—	51.6 ± 2.1
33237	—	44.4 ± 3.9	—	55.4 ± 3.7
33238	3.726 ± 0.115	47.5 ± 2.9	3.550 ± 0.113	54.9 ± 2.9
33239	3.994 ± 0.191	45.5 ± 4.9	4.065 ± 0.182	60.2 ± 4.7
33243	3.786 ± 0.081	50.6 ± 2.1	3.801 ± 0.078	51.5 ± 2.0
33245	3.751 ± 0.134	49.3 ± 3.4	3.751 ± 0.131	46.5 ± 3.3
33246	3.656 ± 0.129	41.9 ± 3.3	3.602 ± 0.130	38.4 ± 3.3
33247	3.710 ± 0.122	46.6 ± 3.1	4.079 ± 0.120	46.7 ± 3.1
33248	3.610 ± 0.110	44.3 ± 2.8	3.750 ± 0.108	46.9 ± 2.7
33249	3.910 ± 0.140	52.9 ± 3.6	3.811 ± 0.136	49.8 ± 3.5
33250	3.597 ± 0.139	49.5 ± 3.5	3.715 ± 0.136	55.5 ± 3.5
33253	3.746 ± 0.154	49.5 ± 3.9	3.743 ± 0.146	46.8 ± 3.7
33254	3.542 ± 0.106	45.4 ± 2.7	3.691 ± 0.103	49.1 ± 2.6

continued on next page

TABLE IV *(continued)*

RHIC Fill	***Blue* beam** $\langle A_N \rangle$ [%]	$\langle P_{beam} \rangle$[%]	***Yellow* beam** $\langle A_N \rangle$ [%]	$\langle P_{beam} \rangle$[%]
33255	3.716 ± 0.126	42.1 ± 3.2	3.891 ± 0.124	48.3 ± 3.2
33256	3.644 ± 0.138	46.2 ± 3.5	3.720 ± 0.135	51.0 ± 3.4
33260	3.526 ± 0.100	54.7 ± 2.6	3.666 ± 0.098	52.8 ± 2.5
33262	3.411 ± 0.129	54.0 ± 3.3	3.719 ± 0.128	53.6 ± 3.3
33263	3.629 ± 0.123	55.1 ± 3.1	3.914 ± 0.121	54.0 ± 3.1
33265	3.834 ± 0.110	56.4 ± 2.8	3.584 ± 0.109	53.7 ± 2.8
33266	3.700 ± 0.107	55.1 ± 2.7	3.569 ± 0.105	49.8 ± 2.7
33267	4.121 ± 0.112	56.6 ± 2.9	3.775 ± 0.107	52.5 ± 2.7
33268	3.846 ± 0.113	61.7 ± 2.9	3.858 ± 0.111	56.0 ± 2.8
33269	3.884 ± 0.153	51.9 ± 3.9	3.678 ± 0.149	56.0 ± 3.8
33270	3.775 ± 0.139	55.4 ± 3.5	3.803 ± 0.136	54.9 ± 3.5
33271	3.674 ± 0.104	51.6 ± 2.7	3.583 ± 0.102	54.5 ± 2.6
33272	3.619 ± 0.195	52.0 ± 5.0	3.919 ± 0.192	54.5 ± 4.9
33273	3.957 ± 0.158	54.9 ± 4.0	3.836 ± 0.153	52.6 ± 3.9
33274	3.536 ± 0.145	54.7 ± 3.7	3.644 ± 0.142	44.3 ± 3.6
33275	4.062 ± 0.115	59.5 ± 2.9	3.670 ± 0.116	54.7 ± 3.0
33276	3.838 ± 0.112	52.7 ± 2.9	3.640 ± 0.111	51.1 ± 2.8
33279	3.790 ± 0.113	54.0 ± 2.9	3.627 ± 0.109	52.3 ± 2.8
33280	3.754 ± 0.113	54.0 ± 2.9	3.775 ± 0.109	52.9 ± 2.8
33281	3.705 ± 0.114	52.3 ± 2.9	3.822 ± 0.111	49.1 ± 2.8
33282	3.681 ± 0.109	55.7 ± 2.8	3.738 ± 0.106	53.4 ± 2.7
33283	3.718 ± 0.115	52.0 ± 2.9	3.777 ± 0.112	52.6 ± 2.8
33284	3.846 ± 0.114	51.2 ± 2.9	3.732 ± 0.112	46.3 ± 2.9
33285	3.425 ± 0.184	55.2 ± 4.7	3.759 ± 0.179	53.2 ± 4.6
33286	3.702 ± 0.105	54.8 ± 2.7	3.736 ± 0.103	50.8 ± 2.6
33287	4.081 ± 0.217	62.3 ± 5.5	3.822 ± 0.213	51.9 ± 5.4
33288	3.646 ± 0.116	52.1 ± 3.0	3.744 ± 0.114	55.0 ± 2.9
33289	3.801 ± 0.221	66.9 ± 5.6	3.785 ± 0.216	52.9 ± 5.5
33290	3.802 ± 0.123	57.0 ± 3.1	3.575 ± 0.120	51.5 ± 3.1
33291	3.845 ± 0.157	53.1 ± 4.0	3.756 ± 0.153	53.8 ± 3.9
33297	3.549 ± 0.120	57.9 ± 3.1	3.661 ± 0.117	54.6 ± 3.0
33298	3.439 ± 0.112	51.9 ± 2.9	3.708 ± 0.109	50.3 ± 2.8
33299	3.723 ± 0.127	60.7 ± 3.2	3.945 ± 0.122	52.6 ± 3.1
33300	3.952 ± 0.137	52.1 ± 3.5	3.936 ± 0.137	54.5 ± 3.5
33304	3.642 ± 0.118	57.4 ± 3.0	3.743 ± 0.113	55.0 ± 2.9
33306	3.696 ± 0.126	51.7 ± 3.2	3.710 ± 0.130	59.3 ± 3.3
33307	3.877 ± 0.086	58.3 ± 2.2	3.897 ± 0.085	55.7 ± 2.2
33308	3.764 ± 0.082	52.4 ± 2.1	3.679 ± 0.082	54.2 ± 2.1
33309	3.729 ± 0.082	50.6 ± 2.1	3.808 ± 0.081	52.1 ± 2.1
33310	3.727 ± 0.078	51.0 ± 2.0	3.616 ± 0.077	51.1 ± 2.0
33311	3.736 ± 0.075	55.0 ± 1.9	3.589 ± 0.074	52.2 ± 1.9
33312	3.691 ± 0.173	52.0 ± 4.4	3.873 ± 0.168	58.6 ± 4.3
Run 22	3.757 ± 0.007	50.4 ± 0.2	3.757 ± 0.007	49.6 ± 0.2
Run 17	3.769 ± 0.006	55.3 ± 0.1	3.765 ± 0.006	56.1 ± 0.1

[1] G. Bunce, N. Saito, J. Soffer, and W. Vogelsang, Ann. Rev. Nucl. Part. Sci. **50**, 525 (2000), arXiv:hep-ph/0007218.

[2] G. Bunce, in *Polarized protons at high-energies - accelerator challenges and physics opportunities. Proceedings, Workshop, Hamburg, Germany, May 17-20, 1999*, edited by A. De Roeck, D. Barber, and G. Radel (1999) pp. 283–288.

[3] A. Zelenski *et al.*, Nucl. Instrum. Meth. A **536**, 248 (2005).

[4] H. Okada *et al.*, Phys. Lett. B **638**, 450 (2006), arXiv:nucl-ex/0502022.

[5] I. G. Alekseev *et al.*, Phys. Rev. D **79**, 094014 (2009).

[6] A. A. Poblaguev, PoS **PSTP2015**, 032 (2016).

[7] A. A. Poblaguev, A. Zelenski, G. Atoian, Y. Makdisi, and J. Ritter, Nucl. Instrum. Meth. A **976**, 164261 (2020), arXiv:2006.08393 [physics.ins-det].

[8] A. A. Poblaguev *et al.*, Phys. Rev. Lett. **123**, 162001 (2019), arXiv:1909.11135 [hep-ex].

[9] V. Schoefer *et al.*, in *Proc. 6th International Particle Accelerator Conference (IPAC'15), Richmond, VA, USA, May 3-8, 2015*, International Particle Accelerator Conference No. 6 (JACoW, Geneva, Switzerland, 2015) pp. 2384–2386, https://doi.org/10.18429/JACoW-IPAC2015-TUPWI060.

[10] V. Ranjbar *et al.*, in *Proc. of International Particle Accelerator Conference (IPAC'17), Copenhagen, Denmark, 14-19 May, 2017*, International Particle Accelerator Conference No. 8 (JACoW, Geneva, Switzerland, 2017) pp. 2188–2190, https://doi.org/10.18429/JACoW-IPAC2017-TUPVA050.

[11] A. V. Fedotov *et al.*, Phys. Rev. Lett. **124**, 084801 (2020).

[12] A. A. Poblaguev, *Waveform dependence on signal amplitude in the RHIC H-Jet polarimeter*, Tech. Rep. BNL-104366-2014-TECH, C-A/AP/505 (Brookhaven National Laboratory, 2014) (unpublished).

[13] A. Poblaguev, E. C. Aschenauer, G. Atoian, K. Eyser, H. C. Huang, Y. Makdisi, W. Schmidke, A. Zelenski, I. Alekseev, and D. Svirida, PoS **PSTP2017**, 022 (2018).

[14] N. H. Buttimore, B. Z. Kopeliovich, E. Leader, J. Soffer, and T. L. Trueman, Phys. Rev. D **59**, 114010 (1999), arXiv:hep-ph/9901339.